The Mysterious Green Streaks Below STEVE

Joshua Semeter[1], Elizabeth MacDonald[2], Michael Hunnekuhl[3], Michael Hirsch[1], Neil Zeller[4]

[1]Department of Electrical and Computer Engineering and Center for Space Physics, Boston University, Boston, MA, USA

[2]NASA, Goddard Space Flight Ctr, Greenbelt, MD 20771 USA.

[3]Eichenweg 15, 30989 Gehrden, Germany

[4]Neil Zeller Photography, Calgary, AB Canada

Key Points:

- Extremely small point-like features are observed within the 'picket fence' STEVE phenomena.
- Such features point to the role of local ionospheric production.
- The features are among the smallest optical features found in the natural airglow or aurora.

Corresponding author: Joshua Semeter, Boston University, 8 St. Mary's St., Boston, MA 02215, jls@bu.edu

Abstract

STEVE (Strong Thermal Emission Velocity Enhancement) is an optical phenomenon of the sub-auroral ionosphere arising from extreme ion drifts. STEVE consists of two distinct components in true-color imagery: a mauve or whitish arc extended in the magnetic east-west direction, and a region of saturated green emission adjacent to the arc, often structured into periodically spaced columns aligned with the magnetic field (the "picket fence"). This work employs high-resolution imagery by citizen scientists in a critical examination of fine scale features within the green emission region. Of particular interest is a narrow "streak" of emission commonly observed underneath and connected to the field-elongated features above. These streaks exhibit identical coloration to other green features in the field of view, consistent with spectroscopic measurement of a common emission spectrum dominated by the metastable oxygen 557.7 nm line. Triangulation of one event found the streak to form in the range of 102−−106 km altitude. The cross-sectional width of another streak was measured to be as small as ∼350 m. In image sequences, the streak is observed to drift toward the main STEVE channel at ∼500 m/s, with evidence for a curved trajectory. The optical signatures are consistent with a drifting point-like excitation source, where the elongation is due to finite exposure (motion blur) and radiative lifetime effects. The source of the 557.7-nm emission is most likely direct excitation of ambient atomic oxygen by suprathermal electrons generated by ionospheric turbulence induced by the extreme electric fields driving STEVE.

1 Introduction

STEVE (Strong Thermal Emission Velocity Enhancement) is a recently identified optical feature in the sub-auroral ionosphere. appearing within a narrow channel of extreme westward ion drifts (MacDonald et al., 2018). The phenomenon was first identified by citizen scientists using consumer camera equipment. In true-color photography STEVE appears as a diffuse arc extended in the East-West direction with color ranging from mauve to gray-white, which is often, but not always, accompanied by ephemeral green features nicknamed "the picket fence". Multi-point triangulation has placed the mauve component at an altitude range of 130–270-km, with picket fence features extending below to as low as ∼95 km (Archer et al., 2019). Conjugate measurements by the SWARM satellites at ∼400 km have detected $B_\perp$ ion velocities approaching 6 km/s in the STEVE channel, with electron temperatures approaching ∼1 eV near the edges (An-

derson, Heelis, & Hanson, 1991a; Nishimura et al., 2019). Initial spectroscopy of STEVE has revealed the mauve color to arise from the oxygen 630-nm red line emission superimposed on a continuum spectrum from ∼400 to ∼700 nm (Gillies et al., 2019). The whitish color is attributed to lower altitude events, where the metastable $O(^1D)$ state responsible for the red line component is collisionally quenched (Liang et al., 2019). The companion picket fence region has been found to be predominently oxygen 557.7-nm green line, with a trace contribution from N_2 first positive emissions (Mende, Harding, & Turner, 2019). The lack of emissions from higher energy N_2^+ transitions has argued against precipitating magnetospheric electrons as the source of the green features (Mende et al., 2019).

This paper considers STEVE's green companion from a morphological point of view. Particular attention is placed on ephemeral "streaks" of green emission commonly observed below, and conjugate to, field-aligned structures comprising the picket fence. Several examples of this feature are shown in Figure 1, as captured in true-color imagery by citizen scientists. In all cases observed thus far, the streaks form on the poleward side of STEVE, exhibit an approximate north-south elongation, and propagate equatorward toward the main STEVE channel. Similar streaks to those shown in Figure 1 are also found embedded in more dynamic displays (e.g., Figure 5), where their motion is somewhat more complcated and their relationship to the magnetic field topology is less clear. Notably, the lifetime of the streaks is sufficiently long (∼10 s) to enable tracking through multiple images, allowing for deconvolution of finite exposure-time effects (motion blur) and spatiotemporal correlation with other features in the field.

In the remainder of this work, we provide an initial examination of the altitude, trajectory, orientation, and dimensions of this feature, followed by some conjecttures about its origin, and connections to broader questions of the picket fence source and the modes of energy dissipation represented by the STEVE phenomenon. This work also suggests new opportunities for the use of photometric imaging as a diagnostic of ionospheric turbulence under extreme conditions.

2 Analysis results

The experimental results in this work were all derived from imagery recorded by citizen scientists using commercially available equipment. The unfamiliar nature of this phenomenon and the unusual views obtained by the photographers make interpretation

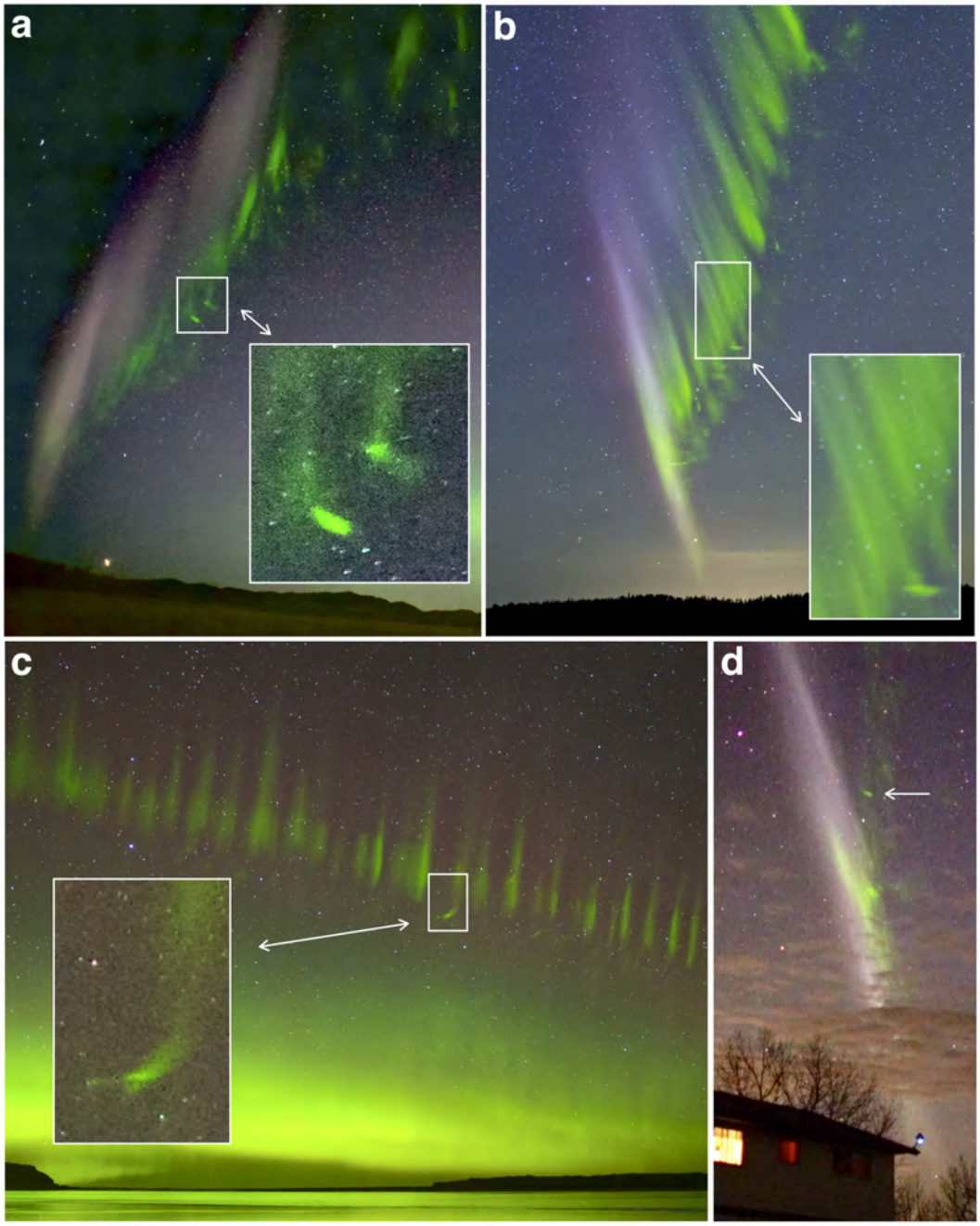

Figure 1. Sample images highlighting STEVE's green component and the mysterious green streaks appearing below the "picket fence" a) 6 May 2018, 11:21:25 LT, 4-s exposure, 51.255°N, 114.701°W (credit: Alexei Chernenkov). b) 13 September 2018, Isle Royale National Park (credit: Shawn Malone). c) 28 March 2017, 15-s exposure (credit: Stephen Voss). d) 6 May 2018, ∼11:19 LT, 33-ms exposure (NTSC video) (credit: Alan Dyer).

with respect to physical hypotheses challenging. Observer perspective, camera exposure times, magnetic field topology, and radiative lifetime effects must all be considered carefully in drawing physical conclusions from these observations. We endeavor to discuss these issues in the context of our analysis. The features of interest are often faint, and the images displayed in this work have been adjusted to enhance contrast. Our findings do not rely on absolute photometric calibration, although that will undoubtedly become an important consideration in future studies.

2.1 Altitude determination

The wide-field perspectives in Figure 1 indicate that the streaks lie underneath other green features. Knowledge of the precise altitude provides an important constraint on candidate source mechanisms. The event in Figure 1a was fortuitously observed from a second location with sufficient separation to enable triangulation. Figure 2 and Figure 1a were from locations (51.255°N, 114.701°W) and (51.267°N, 114.328°W), respectively, at 11:21:25 LT on 6 May 2018. The one-dimensional nature of the streaks allowed the use of end-points as reference points for triangulation. The end-points of the brighter streak are labeled R7 and R8 in Figure 2. Azimuth and elevation calibration was determined using a regional set of reference stars, labeled R3–R6, rather than the full star field. This mitigated uncertainties such as lens distortion and the order of the fitting function, which could introduce errors in triangulation within our small region of interest. An optimization approach was then applied to find the best-fit location of R7 and R8 consistent with star positions. The estimated altitude of streak end-point R1 was in the range 102.2–104.4 km, and R2 was in the range 104.0–106.2 km.

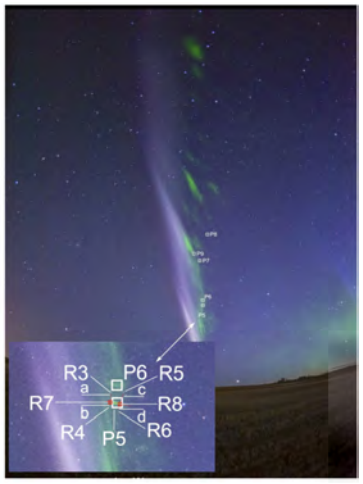

Figure 2. Image of the same event as Figure 1a recorded from location (51.266805°N, 114.328423°W). The pair of images was used for triangulation of the low altitude streaks labeled P5 and P6. The endpoints of P5 are labeled R7 and R8. Reference stars used for elevation and azimuth determination are labeled R3–R5. The altitude was determined to be 102.2 − 104.4 km for R7, and 104.0–106.2 km for R8

2.2 Trajectory

Figure 3 shows a sequence of cropped images at 4-second cadence documenting the formation and evolution of the two streaks highlighted in Figure 1a (courtesy Alexei Chernenkoff). The streaks initially appear as point-like bursts (white arrow in panel a, yellow arrow in panel c), which subsequently elongate along their direction of motion. The trajectory is toward the main STEVE channel in these observations. The elongation of the features is influenced by at least three effects. The first is simple motion blur caused by the 4-s exposure. The second is emission afterglow. As suggested in prior work (Gillies et al., 2019; Mende et al., 2019), the green color is predominantly due to the 557.7 nm line, produced by the metastable $O(^1S - -^3P)$ transmission of atomic oxygen, with radiative lifetime 0.74 s. A moving source of $O(^1S)$ will produce a luminous tail in the 557.7-nm emission due to the finite radiative lifetime. The third effect is spatiotemporal variability in the excitation source itself. Quantifying these effects in this particular image sequence is challenging due to the low sensitivity of the particular equipment used to acquire this sequence. To further examine the dimensions, trajectory, and possible influences of the magnetic field, we turn to a second more dynamic event recorded with greater sensitivity.

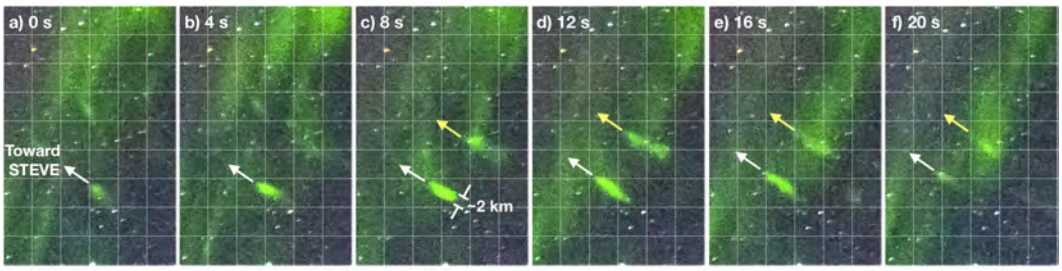

Figure 3. Sequence of 4-second image samples around the time of Figure 1a , showing the general propagation of the streaks toward the main STEVE arc, and their general elongation in the direction of propagation.

Figure 4. STEVE observed with 15-second exposure on 00:33:22 LT on 20 March 2017 from location 51.66 N, 112.91 W. The rectangle is the region detailed at 3.5-second exposure in the image sequence of Figure 5 (courtesy Neil Zeller Photography).

Figure 4 is an image recorded on 20 May 2017 at 00:32 Local Time (LT) from location 51.66 N, 112.91 W at 15-second exposure (courtesy Neil Zeller Photography). In this display, a series of coherent green structures are observed to extend away from the main STEVE channel. The two structures toward the top of the image are composed of periodically spaced bands, each aligned approximately parallel to the main STEVE channel. The overhead zenith direction lies just outside the field of view as indicated, and the mauve-white arc is stretched out along the magnetic east-west direction. The orientation of the green features in Figure 4 is difficult to establish conclusively in this projection.

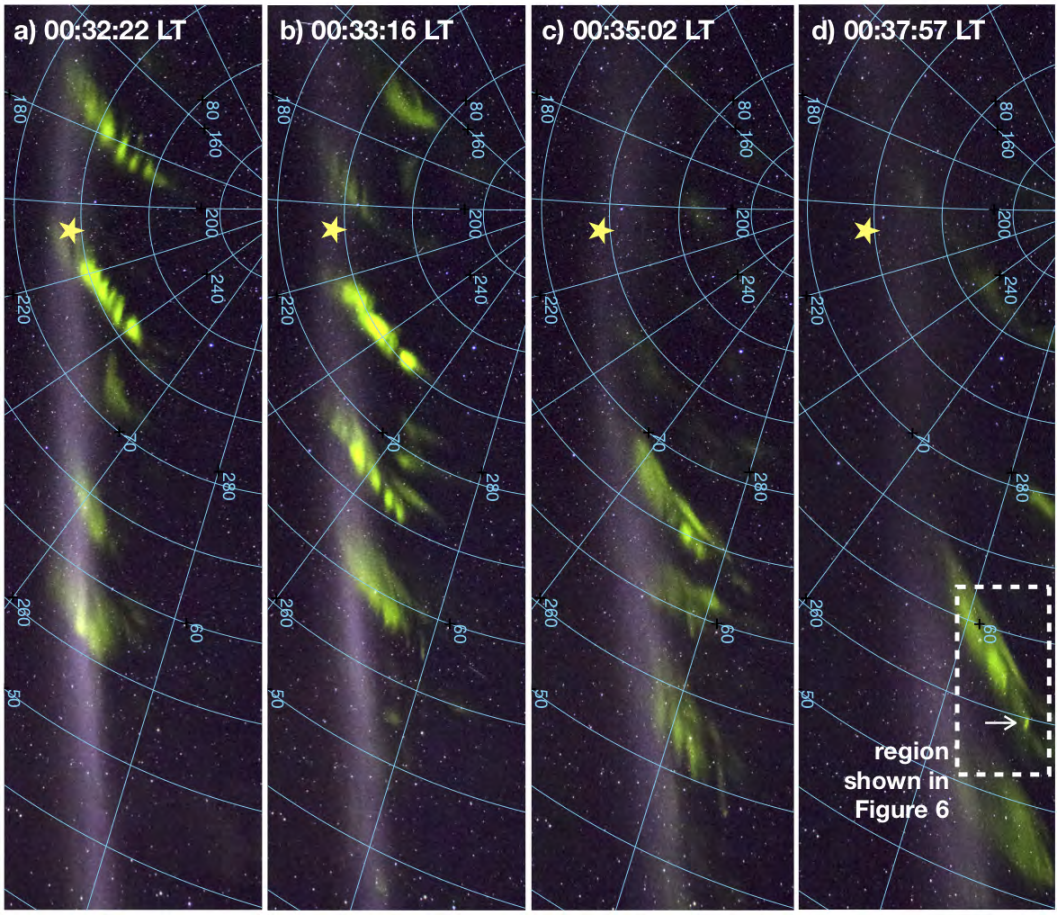

Figure 5. Sample images of dynamic green emissions observed within the rectangular region of Figure 4 on 20 May 2007. Azimuth and elevation contours are shown in blue. The magnetic zenith is indicated by the yellow star.

This event was captured by a second co-located camera with narrower field of view and higher image cadence (3.5-second). Figure 5 shows four selected images from this camera, with local time as indicated. The field-of-view corresponds to the rectangular region in Figure 4. Blue contours indicate geographic azimuth and elevation as determined from star field fitting. The yellow star in each frame indicates the magnetic zenith direction (inclination 73.5°, declination 14°), calculated using the International Geomagnetic Reference Field (IGRF) model (Thébault et al., 2015))

The image samples in Figure 5 were selected to give a sense of how these features varied as they moved westward from near zenith (panel a) to lower elevation (panel d). The individual features changed substantially from frame to frame, indicating that the

phenomena was not fully resolved at 3.5-seconds. The reader is encouraged to view the full image sequences included as supplemental material in time-lapse format.

One feature that remained coherent across multiple frames is the small streak within the dashed box of Figure 5d. This streak has characteristics similar to the streaks in Figures 1 and 3 – I.e., it is the smallest object within the field, it appears below the other features (i.e., lower elevation), and, unlike other features in this sequence, it persisted as a coherent drifting object across several frames.

Figure 5e-i shows the evolution of this feature through five consecutive 3.5-second frames. The field-of-view corresponds to the dashed box in Figure 5d. Panel f duplicates the image from panel e where fiducial marks have been inserted. The white arrows in panel f indicate the location, length, and direction-of-motion of the streak as extracted from the individual panels a–e. The streak is seen to be contiguous from frame to frame (i.e., tip of one arrow lines up with tail of the next). This suggests that it is produced by a drifting point-like source, and that the observed elongation is primarily caused by motion blur and afterglow effects previously discussed. The trajectory is also seen to be slightly curved in this perspective. The curvature is consistent with bending toward the main STEVE channel. This trajectory may have similarities to Figure 1c, where the trace emission behind the streak suggests a drift path that bent into the horizontal plane. The red line inserted in panel f indicates the magnetic field-aligned direction. Its significance will be discussed in Section 2.3.

2.3 Dimensions and Velocity

The high fidelity of Figure 6 allows for a quantitative examination of dimensions and velocities of the streak. Figure 7 shows the relative brightness of the camera's green channel versus distance along its trajectory for each panel (a–e) of Figure 5. The distance scale was computed assuming a constant altitude of 100 km. At its initial appearance, the full-width-at-half-maximum (FWHM) is similar to the separation between the peaks (1.2–1.6 km). This is consistent with a drifting point source subject to motion blur. The streak can also be seen to broaden and develop an asymmetric "tail" behind its trajectory. This is qualitatively consistent with the afterglow effect due to the finite radiative lifetime of the $O(^1S)$ state.

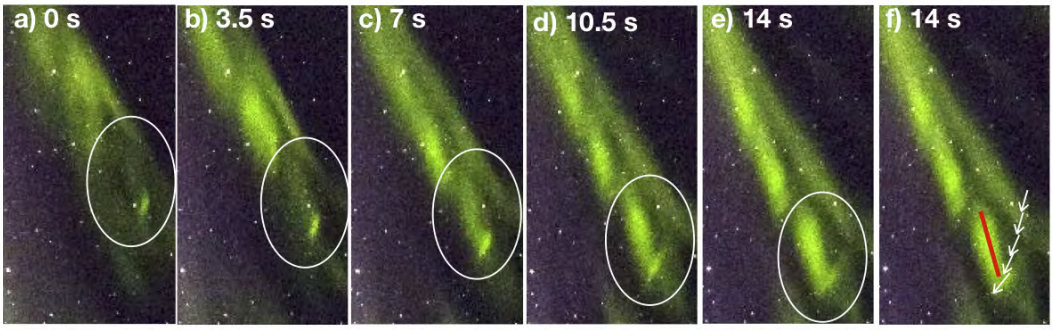

Figure 6. Image sequence at 3.5-second cadence corresponding to the rectangular region in Figure 5d, showing the evolution of an emission streak that persisted in 5 contiguous frames (feature within the white oval). In panel e, the length, orientation, and direction of motion of the streak is shown as a series of vectors. The red line shows the magnetic field-aligned direction superimposed on a features that formed above the streak.

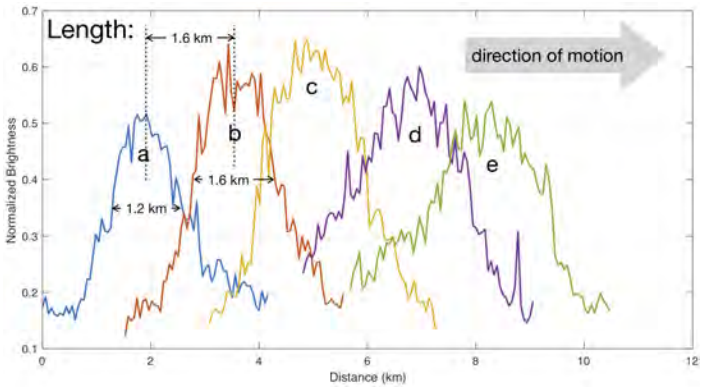

Figure 7. Normalized brightness as a function of distance along the trajectory of the streak feature in Figure 6a-e. The behavior is consistent with a drifting point source. An asymmetry develops as the object moves, consistent with an "afterglow" tail due to the 0.74-s radiative lifetime of the $O(^1S)$ state.

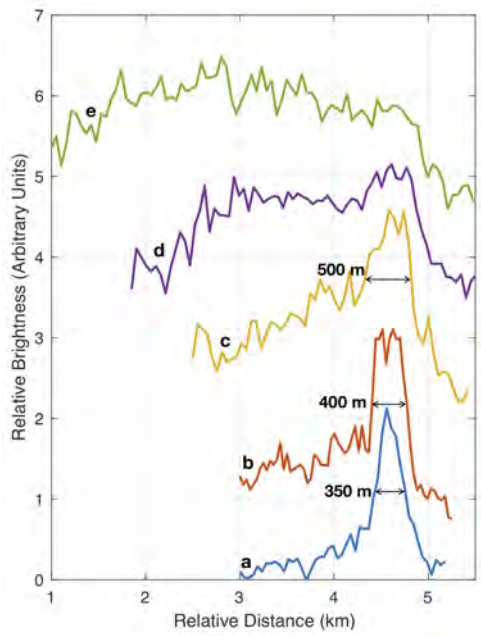

Figure 8. Brightness cuts extracted through the highlighted feature in panels a-e of Figure 6 in a direction aligned with the magnetic field, showing as a line plot the apparent field-aligned elongation of the structure during its lifetime.

Figure 8 shows the evolution of this feature in the direction *transverse* to its propagation. When first observed (curve a) the streak has a cross-sectional FWHM of ∼350 m (assuming, again, an altitude of 100 km). This streak is thus among the smallest optical aeronomical features observed at any latitude. As it evolves through subsequent frames (curves b–e), an extended region of emission is seen to develop to the left (i.e., at higher elevation angle). Some context for this can be obtained by returning to Figure 6. The new region of emission corresponds to a developing magnetic field-aligned feature in the upper part of the encircled region, above the streak. In Figure 6f, a red bar has been inserted to show the magnetic field-line direction projected into the image plane. Magnetic conjugacy of low-altitude streaks and field-aligned features is also observed in the the wide-field image samples of Figure 1. The analysis of Figure 8 provides possible evidence for the contemporaneous development of the low altitude streaks of emission and magnetic field-aligned features above it.

179 ## 3 Discussion

180 True-color images of selected STEVE events obtained by citizen scientists have been
181 used in a critical examination of small-scale features in the green "picket fence" region.
182 Image sequences acquired at 3.5- and 4-second cadence have revealed dynamic sub-kilometer
183 features with varying orientations, dimensions, and motions (Figure 5). Unlike the pe-
184 riodic green columns that inspired the picket fence designation, these features are not
185 extended along magnetic lines of force, and are thus inconsistent with production via en-
186 ergetic particle precipitation. Readers are encouraged to view the time-lapse videos in-
187 cluded as supplemental material to develop their own impression of these unusual fea-
188 tures, as observed in the unique perspectives obtained by citizen scientists.

189 Our analysis has focused on a particular repeatable feature: a narrow "streak" of
190 emission appearing below the picket fence that forms on the poleward side and propa-
191 gates toward STEVE. This feature is noteworthy for several reasons: 1) it is the lowest-
192 altitude and smallest-scale optical feature associated with STEVE; 2) it is observed across
193 a wide range of STEVE events; 3) it often persists for >10 s as a coherent propagating
194 object; 4) it is magnetically conjugate to, and sometimes connected with, overlying field-
195 aligned structures; 5) it exhibits identical coloration to other green features in the field-
196 of-view. Some conjectures based on the initial findings reported herein are discussed be-
197 low.

198 ### 3.1 Source of green line excitation

199 The periodic spacing and magnetic field elongation often observed in the green fea-
200 tures adjacent to STEVE (e.g., Figure 1) have naturally led many to assume production
201 via usual auroral mechanisms – i.e., penetration of magnetospheric electrons with kinetic
202 energy >1 keV (e.g., Gillies et al., 2019; Mishin & Streltsov, 2019; Nishimura et al., 2019).
203 The initial spectroscopic measurements acquired by Gillies et al. (2019) are irreconcil-
204 able with this hypothesis. A careful analysis by (Mende et al., 2019) found the spectrum
205 to be dominated by the metastable oxygen 557.7-nm line (4.19 eV excitation energy, 0.74-
206 s radiative lifetime) but with a trace contribution from prompt N_2 first positive (1P) emis-
207 sions (7.35 eV excitation energy). Entirely absent, however, were contributions from higher
208 energy emissions of N_2^+, often represented in auroral studies by the band-head of the the
209 N_2^+ first negative (1N) group at 427.8 nm (18.75 eV excitation energy). This emission,

produced by collisional ionization and excitation of ambient N_2, must be present for particle penetration to these altitudes. The presence of N_2 1P without N_2^+ 1N has argued for a lack of primary electrons with the requisite >1-keV energy range, rather than a depletion of ambient N_2 (Mende et al., 2019). This finding supported earlier conjectures based on color comparisons (Mende et al., 2019) that the source of the green companion to STEVE is likely direct excitation of oxygen $O(^1S)$ by superthermal electrons energized locally in the ionosphere.

The features examined in this work support this conclusion from a morphological perspective, while also raising new questions. The small scales and variegated orientations of the features highlighted in Figures 1–6 are also irreconcilable with formation by particle precipitation. Analysis of the streak in Figures 6 and 8 are consistent with a drifting point-like source, with cross-sectional size as small as ∼350 meters. Triangulation of a similar feature in Figure 2 has placed this source in the lower ionospheric E-region at 102–106 km, and below other picket fence features in the field. Spectroscopy of the individual streaks is not available. But we would note that the field-elongated structures and the green streaks below them exhibit identical coloration in the true-color imagery, suggesting all green features are arising from a common underlying source mechanism.

3.2 Superthermal electron production

In seeking a source of free energy able to excite oxygen green line features at sub-kilometer scales, it should be noted that the ion drift speeds within STEVE exceed 6 km/s (MacDonald et al., 2018; Nishimura et al., 2019). The patterns and intensities of turbulent heating caused by such supersonic plasma jets in the outer atmosphere are not well known. Additional complications arise from the entanglement of chemistry and electrodynamics; ion velocities in this range are known be associated with rapid conversion from atomic (O^+) to molecular (NO^+) ions (Anderson, Heelis, & Hanson, 1991b), which would impact momentum balance in the channel in a highly nonlinear manner. Under these conditions it is not surprising to find pockets of extreme electron heating.

Some direct evidence for this has been found in conjugate satellite measurements. Nishimura et al. (2019) and Anderson et al. (1991a) have reported measurements by SWARM of a narrow channel of electron heating conjugate to STEVE, with T_e exceeding 8,000 K, and a single-point measurement approaching 12,000 K (>1 eV). The measurements

occurred in a region of depleted plasma densities, and large upward ion velocities, consistent with expected signatures of low-altitude heating. The electron populations are sure to be highly non-Maxwellian, but a distribution with ∼1-eV average energy is expected to have a significant population at the requisite 4.19 eV energy for green line excitation. Candidate mechanisms for production of such populations include the modified two-stream instability (Farley-Buneman instability) (Farley, 1963), the gradient drift instability (Fejer & Kelley, 1980; Simons, Pongratz, & Gary, 1980), or ion-acoustic turbulence (Milan & Lester, 1998). The Farley-Buneman instability has the attraction of leading to potential wells (Milan & Lester, 1998) which could serve to confine the electron heating into small scale structures.

The manifestation of these turbulent processes in airglow or auroral signatures has not been fully considered. The hypothesized photochemical model for production of the 557.7-nm emission is

$$O(^3P) + e(E) \longrightarrow O(^1S) + e(E - 4.19\text{eV}) \quad (1)$$

$$O(^1S) \longrightarrow O(^3P) + h\nu_{557.7} \quad (2)$$

(Itikawa & Ichimura, 1990). Extracting spatiotemporal information about electron heating from imagery of this emission requires careful consideration of source dynamics and radiative lifetime effects, as represented in the space-time perspective of the sensor. It must also be borne in mind that the images only provide information about electrons with energy >4.19 eV (45,0000 K). Lower energy superthermal populations are important and presumably present, but invisible in green-line imagery. A full treatment of these effects is beyond the scope of this work. But a qualitative appreciation of these effects is useful in the evaluation of evidence from citizen science imagery.

3.3 Relation to magnetic field-aligned features

An initial examination of image sequences has provided evidence for connections between the low altitude emission streaks, and magnetic field-aligned features comprising the "picket fence." The evidence is summarized in Figure 9 for the examples used in this study. In each panel, the grayscale image depicts the green channel of the camera, displayed as a negative for ease of annotation. The red arrows highlight features aligned with the magnetic field; the blue arrows indicate the orientation and trajectory of the streaks. Figure 9a is from 3c. At this point, the upper streak is observed to have devel-

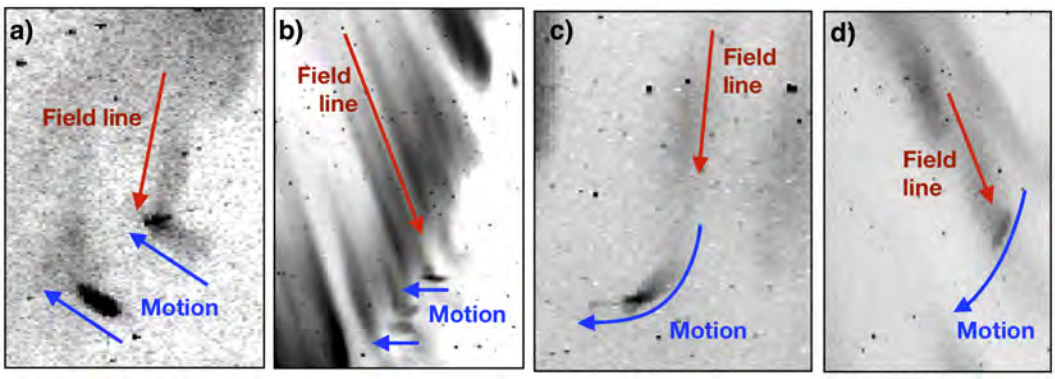

Figure 9. Relationship between magnetic field-aligned features (red) and streak orientation and motion (blue). The images show the green channel of the cameras, displayed as a negative (emissions are dark) a) From Figures 1a and 3c. Blue arrows show the horizontal equatorward direction of motion, as observed in Figures 3a-f. b) From Figure 1b. Blue arrows show the orientation of the streaks in relation to magnetic field direction. c) From Figure 1c. Blue curve highlight the curved shape of the airglow feature which appears to bend into the field-perpendicular equatorward direction. d) From Figure 5g (rotated 90°). Blue curve shows the complete trajectory as extracted from the image sequence in Figures 5e-j.

oped a visible tail extending behind the trailing edge, which is qualitatively consistent with the afterglow effects discussed in Section 2.2. This streak also exhibits evidence of a faint emission column extending above it in the magnetic field-aligned direction. The combination of these effects form an intriguing "L" shape in the image.

Figure 9b is from Figure 1b. Multiple horizontal streaks can be seen conjugate to field-aligned aurora-like structures. Note that the orientation of the streak is not perpendicular to the magnetic field direction, but rather appears to be in the geographically horizontal direction. This would suggest that the orientation and propagation are related to collisional processes (i.e., cross-field mobility), which are organized by mass density, hence altitude, rather than guiding center ($E \times B$) drift (Schunk & Nagy, 2009).

Panels c and d provide some supporting evidence for this conjecture. Panel c (from Figure 1c) shows evidence of a curved tail behind the feature, which bends from the field-parallel direction into the horizontal direction at lower altitudes. If the green line is excited by a drifting source of hot electrons, then the drift would be confined to the $B_{\parallel}$ direction at higher altitudes, but develop an increasing $B_{\perp}$ component at lower altitudes

as the electron cross-field mobility increases, thus allowing the electrons to respond to the poleward directed electric field.

This interpretation is speculative from only a single still image. However, a similarly curved trajectory is observed in Figure 9d. This result was obtained by tracking the feature through multiple frames (Figures 6a-e). The temporal development of a magnetic field-aligned feature above the streak was similarly observed in these frames. This process was summarized in Figure 8, where the cross-sectional width of the streak began with a value of ∼350 m (curve a). As the streak drifted, the emission was obseved to extend upward in the magnetic field-aligned direction.

3.4 Formation of field-aligned features from point sources

One question that arises naturally from the evidence thus far assembled is whether field-aligned "aurora-like" optical features can evolved from point-like sources produced by turbulent heating. Preferential expansion of an isolated plasma population along the magnetic field direction is expected considering the difference in field-parallel versus field-perpendicular mobility (Rishbeth & Garriott, 1969). This effect has been well studied in the context of artificial plasma release experiments (Haerendel & Lüst, 1968), where a cloud of ionized Barium (Ba^+) is observed to rapidly striate across magnetic field lines and elongate along magnetic field lines, forming structures reminiscent of rayed aurora within a few seconds (Simons et al., 1980). The cross-field striation is thought to be caused by the gradient drift instability (Linson & Workman, 1970; Simons et al., 1980). This mechanism is also be plausible here due to the presence of extreme electric fields and extreme density gradients on the edges of the STEVE channel (Nishimura et al., 2019).

In chemical release experiments, the injected plasma was a cold long-lived Barium ion (Ba^+) illuminated by sunlight florescence. In the present situation, the illuminating agent would be superthermal electrons with energy >4.19 eV exciting the oxygen $O(^1S)$ state. In the images sequences of Figures 3 and 6, the excitation source persisted for >10 s, which is long compared with time scales for field-line elongation observed in Barium releases (Simons et al., 1980).

However, based on the limited evidence thus far obtained, it is also possible that the streaks and the picket fence are not causally connected but, rather, represent two distinct responses to the same free energy source. Mende et al. (2019) conjectured that

the magnetic field-aligned features could be produced by wave heating induced by the extreme electric fields in the Sub-auroral ion drift (SAID) region (Streltsov & Mishin, 2003). Fine-scale green emissions at lower conjugate altitudes could be excited by these same extreme fields.

4 Conclusions and Next Steps

The discovery of STEVE has elevated the role of citizen scientists in primary research. In their quest to obtain beautiful imagery of the natural world, photographers have serendipitously discovered a phenomenon overlooked by professional scientists. References to STEVE have since been uncovered in historical literature (Hunnekuhl & MacDonald, 2020), but without its current appreciation as a phenomenon distinct from the aurora and airglow (Gallardo-Lacourt, Liang, Nishimura, & Donovan, 2018).

The low-light monochromatic imaging systems typically employed by professional scientists (Baumgardner, Flynn, & Mendillo, 1993; Eather & Cyril, 1993) embody a particular observational bias. These instruments are designed to observe in specific wavelength bands based on known spectral features in the airglow and aurora. The new millennium saw the proliferation of CMOS-based cameras in the commercial sector. CMOS was a disruptive technology for high resolution, high frame-rate imaging. The level of detail exhibited in Figures 5 and 6) was achieved by exploiting modern commercial CMOS cameras while relaxing the requirement for narrow-band filtering. The results have revealed new structural detail about STEVE, while still retaining sufficient spectral detail to connect these resultts to STEVE discoveries obtained using traditional "scientific grade" instruments.

The appearance of narrow streaks of emission in the lower ionospheric E-region conjugate to, and with identical coloration as, the field-aligned features comprising the STEVE picket fence raises new theoretical questions and presents new observational challenges. First, we cannot yet state with certainty that the spectral signatures across all green features is the same. What is needed are carefully coordinated experiments involving collaborative observations from high frame-rate broad-band cameras of the type employed herein, and similarly high resolution imaging spectrographs of the type employed by (Gillies et al., 2019). Second, if these streaks are caused by turbulent heating related to the extreme electric fields driving STEVE, then we must fill the gap between theoretical pre-

dictions of heating rates to structured excitation of the 4.19-eV $O(^1S)$ state producing the visible features. This will require collaborative efforts that conjoin regional transport modeling (e.g., Zettergren & Semeter, 2012), kinetic plasma simulation (e.g., Oppenheim & Dimant, 2004), and aeronomical modeling of optical emissions (e.g., Solomon, 2017).

Of critical importance going forward will be the aggregation of evidence from multiple sources including citizen scientists. Among the observational gaps that citizen scientists can help fill are: 1) obtaining image sequences at highest possible frame rate; 2) ensuring accurate location, timing, and camera settings are recorded into image metadata; 3) coordinating common-volume observations from multiple locations to enable triangulation and, eventually, three-dimensional tomography of fine scale features within STEVE (Hirsch et al., 2016, e.g.,), 4) engaging with the global community (e.g., Aurorasaurus.org) to share observations.

References

Anderson, P. C., Heelis, R. A., & Hanson, W. B. (1991a, Apr). The ionospheric signatures of rapid subauroral ion drifts. *jgr*, *96*(A4), 5785-5792. doi: 10.1029/90JA02651

Anderson, P. C., Heelis, R. A., & Hanson, W. B. (1991b, Apr). The ionospheric signatures of rapid subauroral ion drifts. *jgr*, *96*(A4), 5785-5792. doi: 10.1029/90JA02651

Archer, W. E., St. -Maurice, J. P., Gallardo-Lacourt, B., Perry, G. W., Cully, C. M., Donovan, E., ... Eurich, D. (2019, Oct). The Vertical Distribution of the Optical Emissions of a Steve and Picket Fence Event. *grl*, *46*(19), 10,719-10,725. doi: 10.1029/2019GL084473

Baumgardner, J. L., Flynn, B., & Mendillo, M. J. (1993, December). Monochromatic imaging instrumentation for applications in aeronomy of the earth and planets. *Optical Engineering*, *32*, 3028-3032. doi: 10.1117/12.149194

Eather, R., & Cyril, L. (1993). *High frequency active auroral research program (HAARP) imager.* (PL-TR-93-2219, Brookline, KeoConsultants, 309 pages.)

Farley, D. T., Jr. (1963, November). A Plasma Instability Resulting in Field-Aligned Irregularities in the Ionosphere. *J. Geophys. Res.*, *68*, 6083. doi: 10.1029/JZ068i022p06083

Fejer, B. G., & Kelley, M. C. (1980). Ionospheric irregularities. *Reviews of Geophysics*, *18*(2), 401–454. Retrieved from http://dx.doi.org/10.1029/RG018i002p00401 doi: 10.1029/RG018i002p00401

Gallardo-Lacourt, B., Liang, J., Nishimura, Y., & Donovan, E. (2018, Aug). On the Origin of STEVE: Particle Precipitation or Ionospheric Skyglow? *GRL*, *45*(16), 7968-7973. doi: 10.1029/2018GL078509

Gillies, D. M., Donovan, E., Hampton, D., Liang, J., Connors, M., Nishimura, Y., ... Spanswick, E. (2019, Jul). First Observations From the TREx Spectrograph: The Optical Spectrum of STEVE and the Picket Fence Phenomena. *GRL*, *46*(13), 7207-7213. doi: 10.1029/2019GL083272

Haerendel, G., & Lüst, R. (1968, nov). Artificial Plasma Clouds in Space. *Scientific American*, *219*(5), 80-92. doi: 10.1038/scientificamerican1168-80

Hirsch, M., Semeter, J., Zettergren, M., Dahlgren, H., Goenka, C., & Akbari, H. (2016, May). Reconstruction of Fine-Scale Auroral Dynamics. *IEEE Transactions on Geoscience and Remote Sensing*, *54*, 2780-2791. doi: 10.1109/TGRS.2015.2505686

Hunnekuhl, M., & MacDonald, E. (2020). Early Ground-Based Work by Auroral Pioneer Carl Stormer on the High-Altitude Detached Subauroral Arcs Now Known as "STEVE". *Space Weather*, *18*(3), e2019SW002384. Retrieved from https://agupubs.onlinelibrary.wiley.com/doi/abs/10.1029/2019SW002384 doi: 10.1029/2019SW002384

Itikawa, Y., & Ichimura, A. (1990, May). Cross Sections for Collisions of Electrons and Photons with Atomic Oxygen. *Journal of Physical and Chemical Reference Data*, *19*(3), 637-651. doi: 10.1063/1.555857

Liang, J., Donovan, E., Connors, M., Gillies, D., St-Maurice, J. P., Jackel, B., ... Chu, X. (2019, December). Optical Spectra and Emission Altitudes of Double-Layer STEVE: A Case Study. *grl*, *46*(23), 13,630-13,639. doi: 10.1029/2019GL085639

Linson, L. M., & Workman, J. B. (1970). Formation of striations in ionospheric plasma clouds. *Journal of Geophysical Research (1896-1977)*, *75*(16), 3211-3219. Retrieved from https://agupubs.onlinelibrary.wiley.com/doi/abs/10.1029/JA075i016p03211 doi: 10.1029/JA075i016p03211

MacDonald, E. A., Donovan, E., Nishimura, Y., Case, N. A., Gillies, D. M.,

Gallardo-Lacourt, B., ... Schofield, I. (2018, Mar). New science in plain sight: Citizen scientists lead to the discovery of optical structure in the upper atmosphere. *Science Advances*, *4*(3), eaaq0030. doi: 10.1126/sciadv.aaq0030

Mende, S. B., Harding, B. J., & Turner, C. (2019, December). Subauroral Green STEVE Arcs: Evidence for Low-Energy Excitation. *grl*, *46*(24), 14,256-14,262. doi: 10.1029/2019GL086145

Milan, S. E., & Lester, M. (1998, Jan). Simultaneous observations at different altitudes of ionospheric backscatter in the eastward electrojet. *Annales Geophysicae*, *16*(1), 55-68. doi: 10.1007/s00585-997-0055-9

Mishin, E., & Streltsov, A. (2019). Steve and the picket fence: Evidence of feedback-unstable magnetosphere-ionosphere interaction. *Geophysical Research Letters*, *46*(24), 14247-14255. Retrieved from `https://agupubs.onlinelibrary.wiley.com/doi/abs/10.1029/2019GL085446` doi: 10.1029/2019GL085446

Nishimura, Y., Gallardo-Lacourt, B., Zou, Y., Mishin, E., Knudsen, D. J., Donovan, E. F., ... Raybell, R. (2019, Jun). Magnetospheric Signatures of STEVE: Implications for the Magnetospheric Energy Source and Interhemispheric Conjugacy. *GRL*, *46*(11), 5637-5644. doi: 10.1029/2019GL082460

Oppenheim, M. M., & Dimant, Y. S. (2004, November). Ion thermal effects on E-region instabilities: 2D kinetic simulations. *Journal of Atmospheric and Solar-Terrestrial Physics*, *66*(17), 1655-1668. doi: 10.1016/j.jastp.2004.07.007

Rishbeth, H., & Garriott, O. (1969). *Introduction to ionospheric physcis*. Academic Press.

Schunk, R. W., & Nagy, A. (2009). *Ionospheres: Physics, Plasma Physics, and Chemistry*. Cambridge, United Kingdom: Cambridge University Press; 2 edition.

Simons, D. J., Pongratz, M. B., & Gary, S. P. (1980, Feb). Prompt striations in ionospheric barium clouds due to a velocity space instability. *jgr*, *85*(A2), 671-677. doi: 10.1029/JA085iA02p00671

Solomon, S. C. (2017). Global modeling of thermospheric airglow in the far ultraviolet. *Journal of Geophysical Research: Space Physics*, *122*(7), 7834-7848. Retrieved from `https://agupubs.onlinelibrary.wiley.com/doi/abs/10.1002/2017JA024314` doi: 10.1002/2017JA024314

Streltsov, A. V., & Mishin, E. V. (2003). Numerical modeling of localized

electromagnetic waves in the nightside subauroral zone. *Journal of Geophysical Research: Space Physics*, *108*(A8). Retrieved from `https://agupubs.onlinelibrary.wiley.com/doi/abs/10.1029/2003JA009858` doi: 10.1029/2003JA009858

Thébault, E., Finlay, C. C., Beggan, C. D., Alken, P., Aubert, J., Barrois, O., ... Zvereva, T. (2015). International geomagnetic reference field: The 12th generation international geomagnetic reference field - The twelfth generation. *Earth, Planets and Space*, *67*(1). doi: 10.1186/s40623-015-0228-9

Zettergren, M., & Semeter, J. (2012). Ionospheric plasma transport and loss in auroral downward current regions. *J. Geophys. Res.*. doi: doi:10.1029/2012JA017637,inpress